Journal of Marine Research, 63, 601–621, 2005

Solute-specific pore water irrigation: Implications for chemical cycling in early diagenesis

by Christof Meile[1], Peter Berg[2], Philippe Van Cappellen[3] and Kagan Tuncay[4]

ABSTRACT

In one-dimensional (1D) early diagenetic models, bioirrigation is typically represented by a nonlocal mass transfer or bioirrigation coefficient, α. Usually, all pore water species are assigned the same α. Here, we show that this assumption can lead to significant errors in estimates of bioirrigation intensities. Using a simplified early diagenetic reaction network, we compute the 3D concentration fields of major pore water species around a vertical burrow, as well as the solute fluxes across the burrow wall. From these results, corresponding 1D vertical α profiles are derived. The α profiles show pronounced differences from one solute to another. Dissolved O_2 systematically exhibits the highest α values, while fast oxygenation kinetics near the burrow wall result in near-zero α values for aqueous Fe^{2+}. For nitrate, use of a species-averaged α profile may even lead to an erroneous prediction of the direction of the irrigation flux across the water-sediment interface. The large differences in α profiles reflect the variable effects of biogeochemical processes on pore water concentration fields of reactive solutes near the burrow wall. Even for inert solutes, however, determination of α can be ambiguous. Transient simulations mimicking the intrusion into the sediment of an inert tracer during an incubation experiment yield apparent mixing intensities that depend on the incubation time.

1. Introduction

The pumping activity of tube-dwelling fauna, or bioirrigation, may contribute significantly to pore water transport in aquatic sediments and to solute exchange fluxes with the overlying water column (Aller, 1983, 2001; Meile and Van Cappellen, 2003). Enhanced solute transport in sediments affects the distributions of reactants and metabolites, the location and magnitude of early diagenetic reactions, and the resident microbial community structure (e.g., Steward *et al.,* 1996; Marinelli *et al.,* 2002). For example, increased O_2 supply by irrigation may enhance the breakdown of sedimentary organic matter (Kristensen, 2000), while the cycling of redox sensitive elements, notably nitrogen, sulfur and iron, may be intensified by the presence and active flushing of burrows (Pelegri *et al.,*

1. Department of Marine Sciences, The University of Georgia, Athens, Georgia, 30602, U.S.A. ***email: cmeile@uga.edu***
2. Department of Environmental Sciences, University of Virginia, Charlottesville, Virginia, 22904, U.S.A.
3. Faculty of Geosciences and Geochemistry, Utrecht University, 3508 TA Utrecht, The Netherlands.
4. Department of Chemistry, Indiana University-Bloomington, Bloomington, Indiana, 47405, U.S.A.

1994; Mayer *et al.,* 1995; Gribsholt *et al.,* 2003; Gilbert *et al.,* 2003; Nielsen *et al.,* 2003, 2004).

Although irrigation is a complex three-dimensional phenomenon (Aller, 1980), it is usually approximated in one-dimensional (1D) reactive transport models by a nonlocal source-sink function, originally put forward by Boudreau (1984) and Emerson *et al.* (1984). This function expresses the removal or supply of a solute by irrigation at a given sediment depth, z, as $\alpha(C_0 - \bar{C})$, where α is the irrigation coefficient, C_0 the bottom water concentration, and $\bar{C}$ the horizontally averaged concentration at depth z. The nonlocal exchange description is the standard formulation for bioirrigation adopted in early diagenetic modeling (see, for example, Boudreau, 1996; Van Cappellen and Wang, 1996; Wang and Van Cappellen, 1996; Berg *et al.,* 1998; Fossing *et al.,* 2000; Furukawa *et al.,* 2000; Meile *et al.,* 2001; Furukawa *et al.,* 2001; Koretsky *et al.,* 2002; Berg *et al.,* 2003), as it corresponds to the horizontal averaging in one-dimensional models. The function requires only one depth-dependent parameter, α, which lumps together the effects of burrow geometry, distribution and flushing into a single mass transfer or exchange coefficient. The model simplicity is a significant advantage when only limited information on the irrigation regime is available. Values of α as a function of depth are typically estimated by fitting models to measured tracer distributions (Martin and Sayles, 1987; Martin and Banta, 1992), or through inverse approaches where measured depth profiles of solute concentrations and corresponding net reaction rates are optimized simultaneously (Fossing *et al.,* 2000; Meile *et al.,* 2001). Recently, a stochastic method for estimating α profiles directly from benthic burrow networks has also been presented (Koretsky *et al.,* 2002).

In 1D multicomponent early diagenetic model simulations, it is commonly assumed that the same α applies to all solutes. Several authors have questioned the appropriateness of using a generic nonlocal exchange description, however. For instance, Aller (2001) identified reaction zonation around burrows, transient concentrations in burrow water, and solute-specific diffusion rates across burrow walls as possible sources of variability in α values. Berg *et al.* (2003) further suggested that differences in the reactive behavior near burrow walls may affect solute transfer between bulk sediment and burrows. For example, dissolved inorganic carbon (DIC) is predominantly produced in the sediment matrix by organic matter mineralization. The resulting build-up of DIC in the sediment matrix causes transport by molecular diffusion toward the sediment-water interface, as well as toward flushed burrows (Fig. 1A). In this case, the nonlocal source-sink function $\alpha(C_0 - \bar{C})$ correctly predicts the removal of DIC to the water column. The same function would similarly predict a benthic efflux of Fe^{2+}, which is also produced within the anaerobic sediment matrix (Fig. 1B). In contrast to DIC, however, Fe^{2+} reacts rapidly with O_2, which diffuses out of the burrows. Instead of being released into burrows and exported to the water column, Fe^{2+} oxidatively precipitates just outside the burrow walls (Balzer, 1982; Sundby *et al.,* 1989). A unique irrigation coefficient is unlikely to capture these very different responses of DIC and Fe^{2+} to irrigation. To account for these differences in 1D

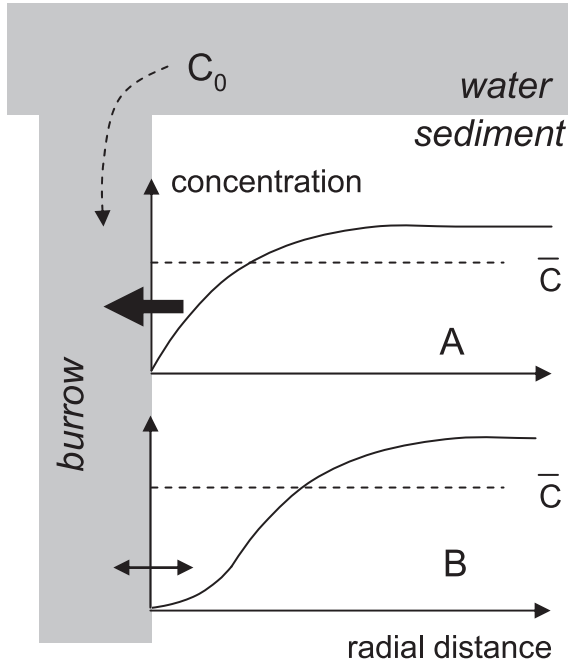

Figure 1. Biogeochemical reactivity and bioirrigation: contrasting radial concentration distributions of two pore water species around a well-irrigated burrow. (A) The solute is produced in the sediment matrix and diffuses toward the burrow without undergoing further reaction. Transport across the burrow wall and subsequent evacuation to the overlying water column is driven by the much lower solute concentration in the burrow, relative to that in the sediment. (B) The solute is produced in the sediment matrix but reacts rapidly with a solute diffusing from the burrow into the surrounding sediment matrix. As a result, little solute reaches the burrow, despite the favorable concentration difference ($C_0 - \bar{C}$), where $\bar{C}$ is the horizontally averaged solute concentration in the sediment matrix. Modified from Berg *et al.* (2003).

reactive transport calculations, solute-specific α values should be assigned (Berg *et al.,* 2003).

This paper examines the role of reactions and reaction rate distributions on the supply or removal of pore water solutes by faunal burrows, by comparing a 3D representation of an irrigated sediment to a horizontally averaged, 1D representation. Small-scale 3D concentration and rate distributions around a burrow are computed with a multicomponent reactive transport model that includes a simplified early diagenetic reaction network. From these 3D distributions, solute fluxes across burrow walls and laterally averaged concentrations and rates are calculated for a number of diagnostic pore water constituents. The resulting average concentration profiles are then used to derive equivalent 1D irrigation coefficients for the various solute species. The approach also provides a means to compare apparent 1D reaction rates to their laterally averaged microscopic equivalents.

2. Model description

a. Background

A major breakthrough in the quantitative treatment of pore water irrigation was the introduction by Aller of the so-called tube model in which the burrow network is approximated as a system of equally spaced, vertical cylinders of uniform size (Aller, 1980). In this model, bioirrigation results from diffusive exchanges between the sediment matrix and perfectly flushed burrows. The latter condition implies that the composition of the burrow solution is identical to that of the overlying bottom water. The determining factors for the irrigation intensity are therefore the amount of burrow surface area in the irrigated portion of the sediment, the radial pore water concentration gradients at the burrow-sediment interface, and the sediment diffusion coefficients of the solutes of interest. For simple zeroth or first order reaction kinetics, analytical solutions describing the concentration gradients of reactive solutes around the burrows can be derived. These solutions have successfully reproduced measured depth profiles of a number of reactive solutes, including ammonium, sulfate and silica (Aller, 1980).

Another significant breakthrough was the demonstration by Boudreau (1984) that, under certain conditions, the 1D nonlocal exchange model is equivalent to the radially-integrated form of Aller's tube model. In order to relate the irrigation coefficient α to the spacing and size of the burrows, Boudreau used a Taylor series expansion of the radial concentration profile in the sediment matrix. A formal relationship emerges when the radial concentration gradient at the burrow wall can be approximated by the difference between the burrow water concentration and the average concentration in the sediment, $\bar{C}$, divided by an *a priori* unknown length scale. Despite this restriction, the establishment of a formal relationship between the phenomenological 1D nonlocal exchange model and the mechanistic tube model bolstered the implementation of the simple nonlocal exchange description of irrigation in 1D early diagenetic models.

Building on the equivalence of the two bioirrigation models, Koretsky *et al.* (2002) derived irrigation coefficients using stochastic simulations of burrow networks, from which depth distributions of burrow surface areas were obtained. For sulfate, the concentration gradients at the burrow walls were estimated from measured depth profiles of net sulfate reduction rates. For O_2, reaction rates at the burrow-sediment interface were assumed to be similar to those at the sediment-water interface (SWI). The radial O_2 concentration gradients were then estimated from measured vertical O_2 microprofiles, applying a volumetric correction for the transformation from planar to radial geometry. The predicted irrigation coefficients were in good agreement with values obtained by fitting measured concentration profiles with a 1D early diagenetic reactive transport model. However, the results also highlighted substantial differences between the irrigation coefficients of O_2 and sulfate.

In the present study, no *a priori* assumption is made concerning the concentration gradients of pore water solutes near the burrow walls. Rather, solute concentration fields around burrows are calculated explicitly using an early diagenetic reaction network.

Bioirrigation coefficients, α, are then determined by matching the computed diffusive fluxes across burrow walls with the corresponding 1D nonlocal model representation. This approach is applied to the simple burrow network of Aller's tube model.

b. Bioirrigation model

Because of the radial symmetry in Aller's tube model, the concentration fields of solute species are defined by the following 2D mass conservation equation:

$$\phi \frac{\partial C}{\partial t} = \frac{1}{r}\frac{\partial}{\partial r}\left(r\phi D_s \frac{\partial C}{\partial r}\right) + \frac{\partial}{\partial z}\left(\phi D_s \frac{\partial C}{\partial z}\right) + R \quad (1)$$

where C is the solute concentration, D_s is the molecular diffusion coefficient, D_{mol}, corrected for sediment tortuosity via $D_s = D_{mol}/(1 - \ln(\phi^2))$ (Boudreau, 1997), ϕ is porosity, R is the sum of all reaction rates acting upon C, and z and r correspond to the vertical and radial directions, respectively.

Eq. (1) is solved numerically by dividing the model domain into small control volumes (Patankar, 1980). To compute the time evolution of the concentration fields, a Euler time stepping scheme is adopted. Integrating Eq. 1 in the vertical and radial directions over a control volume (i, j) yields

$$\phi_{i,j}\frac{C_{i,j}^{new} - C_{i,j}}{\Delta t} = \frac{\left(\left(r\phi D_s \frac{\partial C}{\partial r}\right)_{i+(1/2),j} - \left(r\phi D_s \frac{\partial C}{\partial r}\right)_{i-(1/2),j}\right)}{r_i \Delta r_i} + \frac{\left(\left(\phi D_s \frac{\partial C}{\partial z}\right)_{i,j+(1/2)} - \left(\phi D_s \frac{\partial C}{\partial z}\right)_{i,j-(1/2)}\right)}{\Delta z_j} + R_{i,j} \quad (2)$$

where r_i and z_j denote the radial and vertical positions of the center of the control volume, Δz_j and Δr_i are its vertical and radial dimensions, and the $\pm$ ½ indices correspond to the surfaces separating adjacent control volumes. The terms with concentration gradients express the diffusive mass exchange between adjacent volumes. The radial and vertical concentration gradients are discretized by estimating concentrations at the separating surfaces from the exact solution of the steady-state 1D diffusion equation in vertical or radial direction, assuming constant medium properties (D, ϕ) in each control volume (for a detailed example of the implementation of this numerical scheme, see Rysgaard and Berg (1996)). Diffusion and reaction rates are calculated using the last known concentrations. Grid spacing is variable, with the highest resolution (on the order of 1 mm) near the burrow wall and sediment-water interface (SWI), and coarser resolution elsewhere. The computational domain extends down to 1 m below the SWI, although significant concentration changes are restricted to the upper 25 cm of the sediment. Zero flux boundary conditions

Table 1. Reaction network. C_{org} represents organic matter of composition $(CH_2O)_a(NH_3)_b$; the Redfield ratio $a{:}b = 106{:}16$ is assumed in the simulations. $R(z)$ corresponds to the total organic carbon oxidation rate, K_m^i and K_{sol}^i represent half-saturation concentrations and mineral solubility products, respectively. Rate expressions and rate parameters are based on Wang and Van Cappellen (1996) and Furukawa (2001). Also listed are the molecular diffusion coefficients and concentrations at the SWI of the reactive solutes considered in the model.

Reactions & rate expressions
aerobic respiration: $R_1 = R(z) \cdot O_2/(K_m^{O_2} + O_2)$ $C_{org} + aO_2 + bH^+ \rightarrow aCO_2 + bNH_4^+ + aH_2O$
denitrification: $R_2 = (R(z) - R_1) \cdot NO_3^-/(K_m^{NO_3^-} + NO_3^-)$ $C_{org} + \frac{4a}{5}NO_3^- + \left(\frac{4a}{5} + b\right)H^+ \rightarrow aCO_2 + \frac{2a}{5}N_2 + bNH_4^+ + \frac{7a}{5}H_2O$
iron reduction: $R_3 = (R(z) - R_1 - R_2) \cdot Fe(OH)_3/(K_m^{Fe(OH)_3} + Fe(OH)_3)$ $C_{org} + 4aFe(OH)_3 + (7a + b)CO_2 \rightarrow 4aFe^{2+} + bNH_4^+ + (8a + b)HCO_3^- + (3a - b)H_2O$
sulfate reduction: $R_4 = R(z) - R_1 - R_2 - R_3$ $C_{org} + \frac{a}{2}SO_4^{2-} + bCO_2 + bH_2O \rightarrow \frac{a}{2}H_2S + bNH_4^+ + (a + b)HCO_3^-$
nitrification: $R_5 = k_{nitri} \cdot NH_4^+ \cdot O_2$ $NH_4^+ + 2O_2 + 2HCO_3^- \rightarrow NO_3^- + 2CO_2 + 3H_2O$
iron oxidation with O_2: $R_6 = k_{feox} \cdot Fe^{2+} \cdot O_2$ $Fe^{2+} + 0.25O_2 + 2HCO_3^- + 0.5H_2O \rightarrow Fe(OH)_3 + 2CO_2$
sulfide oxidation with O_2: $R_7 = k_{sox} \cdot TS \cdot O_2$ $HS^- + 2O_2 + 2HCO_3^- + H^+ \rightarrow SO_4^{2-} + 2CO_2 + 2H_2O$
sulfide oxidation with $Fe(OH)_3$: $R_8 = k_{soxfe} \cdot TS \cdot Fe(OH)_3$ $HS^- + 8Fe(OH)_3 + 15HCO_3^- + 30H^+ \rightarrow SO_4^{2-} + 8Fe^{2+} + 15CO_2 + 35H_2O$
FeS precipitation (if oversaturated): $R_9 = k_{prec}^{FeS} \cdot \left(\frac{Fe^{2+} \cdot HS^-}{K_{sol}^{FeS} \cdot \{H^+\}} - 1\right)$ $Fe^{2+} + HS^- \rightarrow FeS + H^+$
$FeCO_3$ precipitation (if oversaturated): $R_{10} = k_{prec}^{FeCO_3} \cdot \left(\frac{Fe^{2+} \cdot CO_3^{2-}}{K_{sol}^{FeCO_3}} - 1\right)$ $Fe^{2+} + CO_3^{2-} \rightarrow FeCO_3$
Parameters: $R(z) = \frac{R_0}{a}e^{-\beta z}$; $R_0 = 2.5 \times 10^{-6}$ mol m^{-3} s^{-1}; $\beta = 10$ m^{-1} $Fe(OH)_3(z) = FeOx_0 \cdot e^{[(\ln(0.1)/0.075)z]} \cdot \rho_{FeOx}(1-\phi)/\phi$; $FeOx_0 = 100$ μmol g^{-1}; $\rho_{FeOx} = 2.5$ kg dm^{-3} $K_m^{O_2} = 20$ μM; $K_m^{NO_3^-} = 5$ μM; $K_m^{Fe(OH)_3} = 65$ μmol g^{-1} $k_{nitri} = 1.6 \times 10^{-4}$ mol^{-1} m^3 s^{-1}; $k_{feox} = 4.4 \times 10^{-3}$ mol^{-1} m^3 s^{-1} $k_{sox} = 5.1 \times 10^{-6}$ mol^{-1} m^3 s^{-1}; $k_{soxfe} = 2.5 \times 10^{-7}$ mol^{-1} m^3 s^{-1} $k_{prec}^{FeS} = 6.3 \times 10^{-6}$ mol m^{-3} s^{-1}; $K_{sol}^{FeS} = [Fe^{2+}][HS^-]/\{H^+\} = 6.3 \times 10^3$ mol^2 m^{-6} $k_{prec}^{FeCO_3} = 6.3 \times 10^{-5}$ mol m^{-3} s^{-1}; $K_{sol}^{FeCO_3} = [Fe^{2+}][CO_3^{2-}] = 1.56 \times 10^{-4}$ mol^2 m^{-6} $\phi = 0.75$ (bulk sediment); pH = 7

Table 1. (Continued)

species	D_{mol} ($m^2\ s^{-1}$)	C_0 (mM)	Rate
O_2	1.82×10^{-9}	0.228	$-a \cdot R_1 - 2 \cdot R_5 - 0.25 \cdot R_6 - 2 \cdot R_7$
NO_3^-	1.53×10^{-9}	0.015	$-4a/5 \cdot R_2 + R_5$
NH_4^+	1.57×10^{-9}	0	$b \cdot (R_1 + R_2 + R_3 + R_4) - R_5$
N_2	1.58×10^{-9}	0.67	$2a/5 \cdot R_2$
SO_4^{2-}	0.87×10^{-9}	28	$-a/2 \cdot R_4 + R_7 + R_8$
TS	1.50×10^{-9}	0	$a/2 \cdot R_4 - R_7 - R_8 - R_9$
DIC	0.92×10^{-9}	1.82	$a \cdot (R_1 + R_2 + R_3 + R_4) - R_{10}$
Fe^{2+}	0.41×10^{-9}	0	$4a \cdot R_3 - R_6 + 8 \cdot R_8 - R_9 - R_{10}$
tracer	1×10^{-9}	1	0

are imposed at the sides and bottom of the computational domain. Solute concentrations at the SWI are assigned fixed values (C_0).

Simulations are carried out over a cylindrical domain of 5 cm radius, with a burrow at its center. The burrow is 15 cm deep and has a radius of 2.5 mm. The selected burrow spacing corresponds to a density of 127 burrows per m^2, a low to mid-range value for coastal marine environments (Aller, 1980; 2001; Koretsky *et al.,* 2002). The reactions included in the model are listed in Table 1, together with the corresponding rate expressions. The reaction parameters are based on the studies of Wang and Van Cappellen (1996) and Furukawa *et al.* (2001), who relied on data from coastal marine sediments for parameter calibration. Although simplified, the reaction network accounts for the main features of the early diagenetic cycles of C, N, O, S and Fe. The kinetic scheme describing organic matter breakdown reproduces the well-known sequence of utilization of terminal electron acceptors in the order of decreasing free energy yield. Because the present study focuses on the impact of burrowing macrofauna on solute transport (bioirrigation), only the dissolved concentrations are explicitly solved using Eq. (1). The total rate of organic carbon oxidation is imposed as an exponentially decreasing function of depth. Similarly, a fixed distribution of the concentration of reactive iron(III)(hydr)oxides with depth is imposed (Table 1). Precipitation of iron sulfide and carbonate acts as sinks for C, Fe and S.

Simulations are performed for both permanently and intermittently flushed conditions. In the latter case, 10 minutes of flushing are followed by a 20-minute resting period (Boudreau and Marinelli, 1993), or flushing is induced when the O_2 concentration in the burrow drops below 20 μM (Brendel, 1995). During flushing the concentrations inside the burrow are equal to the values imposed at the SWI, C_0. During the resting period, the concentrations in the burrow change as a result of diffusion from or to the sediment matrix. Simulations with permanent flushing are run to steady state, while for intermittent flushing they are continued until the transient concentration

fields no longer change from one flushing cycle to the next. In separate model runs, the progressive intrusion of a conservative tracer into the sediment during a core incubation experiment is simulated. Initially, the concentration of the inert species is set to 0 in the sediment. The concentration in the overlying water is assumed to remain constant, with a value equal to 1.

In the model, reaction processes are restricted to the sediment matrix. Thus, the effects of macrofaunal metabolism on burrow water composition are not taken into consideration (Heip *et al.,* 2001). Other processes and effects that are not represented in the model are variations in diffusion coefficients due to the presence of burrow linings (Aller, 1983), advective flow in the sediment caused by burrow flushing, burrow construction and infilling, or variable burrow morphologies. Therefore, the model results primarily address the role of contrasting biogeochemical reactivities on the bioirrigation intensities of pore water solutes, under conditions representative of a coastal marine depositional environment.

c. 1D bioirrigation coefficients

The numerical solution of Eq. (1) for the suite of solute species considered (Table 1) yields the radially symmetric 3D distributions of concentrations and reaction rates in the burrowed sediment. These distributions are then used to derive corresponding 1D irrigation coefficient profiles. Equating the rate of irrigation (R_{irr}) of the radially symmetric tube model and the 1D nonlocal exchange description for a species m yields:

$$R_{irr} = -\phi D_m \left.\frac{\partial C_m}{\partial r}\right|_b \cdot \frac{A_b}{V} = \alpha_m \phi (C_0 - \bar{C}_m) \tag{3}$$

where A_b and V are the burrow wall area and volume of sediment within depth interval [z, $z + \Delta z$] of the model domain. The concentration gradient in Eq. (3) is calculated at the burrow-sediment interface. The irrigation coefficient α is assumed to be time-invariant, and fluxes across the burrow wall for intermittent flushing scenarios are averaged over a flushing cycle.

Through Eq. (3) the bioirrigation coefficient α is linked to the bottom water concentration C_0. The traditional interpretation of α invokes efficient and continuous flushing so that the concentration inside the burrow remains equal to that of the overlying water C_0. The concentration difference ($C_0 - \bar{C}$) then represents the driving force for solute diffusion across the burrow wall, at all depths. In reality, the chemical composition inside inhabited burrows may deviate significantly from that at the SWI (e.g., Brendel, 1995; Meile *et al.,* 2003). In particular, periodic flushing leads to variations in the solute concentration inside the burrow. Such variability may have a much larger effect on the concentration gradient at the burrow wall than on the average concentration within a given sediment layer. Therefore, variations in the burrow water concentration mainly propagate into the calculated value of α (Eq. 3; Koretsky *et al.,* 2002). The magnitude of this effect is explored here by comparing continuous and periodic flushing scenarios.

Experimentally, α values are often constrained by performing sediment incubation experiments, where an unreactive substance is added to the overlying water. One approach consists in deriving nonlocal mixing intensities from the measured drop in tracer concentration in enclosed bottom water during a benthic chamber deployment (e.g., Rao and Jahnke, 2004). Alternatively, the tracer is added to the overlying water in a core incubation experiment (e.g., Martin and Banta, 1992). The pore water tracer distribution is then measured after a given incubation time, and a value of α is determined by fitting the measured tracer profile to the transport equation:

$$\frac{\partial C}{\partial t} = D\,\frac{\partial^2 C}{\partial z^2} + \alpha(C_0 - C). \tag{4}$$

Here, a tracer core incubation experiment is mimicked by laterally averaging the tracer concentrations in the tube model simulations, for variable incubation times. For each incubation time, an irrigation coefficient is determined by least square fitting of the concentration profile obtained with Eq. (4) to the average concentration depth profile. A constant tracer concentration is imposed at the sediment-water interface and a no gradient condition is applied as lower boundary. The value of α is assumed constant in the burrowed portion of the sediment, and 0 below.

3. Results and discussion

a. Concentration fields

The simulated solute concentration fields exhibit distinct vertical and radial patterns, with redox transitions associated with the SWI and the burrow wall (Fig. 2). The general features of the concentration fields are similar for the permanently and intermittently flushed scenarios indicating that, on time scales of hours or less and with diffusion as the main transport process, perturbations of the concentrations are restricted to the close vicinity of the burrow. The horizontally-averaged depth profiles exhibit the typical succession of redox-sensitive solutes (Figs. 2A and 2F). The presence of burrows, however, creates significant vertical overlap between the average concentration profiles of oxidized and reduced solute species.

Concentrations of O_2 drop rapidly away from the SWI and burrow wall (Fig. 2B). Intense O_2 consumption is due to both aerobic degradation of organic matter and the oxidation of ferrous iron, sulfide and ammonium. Nitrate distributions resemble those of O_2, except that the lateral penetration of NO_3^- away from the burrow increases with increasing depth (Fig. 2C). This reflects the decreasing total rate of organic matter oxidation imposed in the simulations. As a consequence, the rate of consumption of nitrate, which in the reaction network considered only occurs via denitrification coupled to organic carbon oxidation, also decreases with depth.

In the topmost few centimeters, an accumulation of aqueous Fe^{2+} is observed away from the burrow (Fig. 2E), in qualitative agreement with the microelectrode measurements of

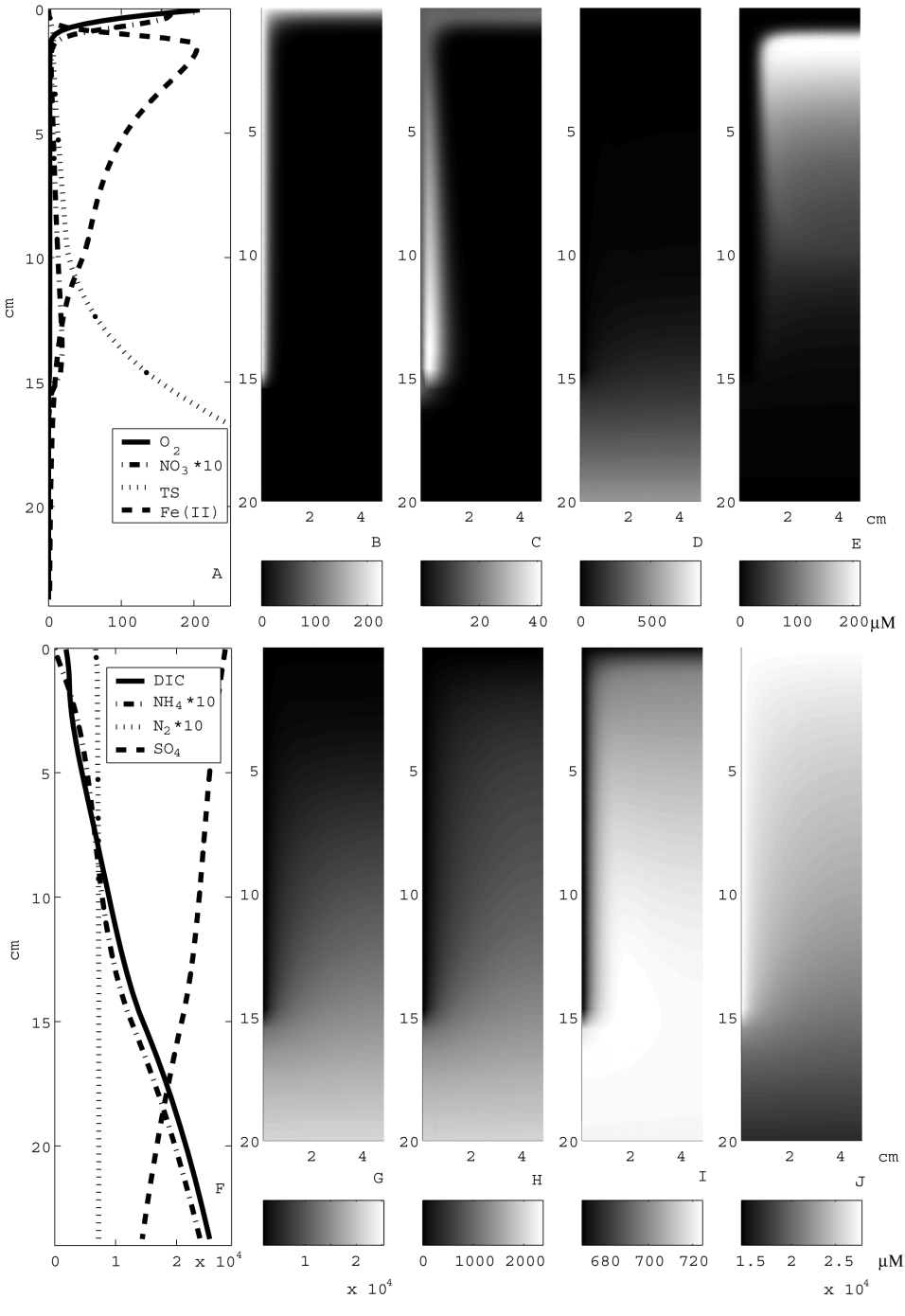
cm
O2
NO3 *10
TS
Fe(II)
A
B
C
D
E
cm
μM
DIC
NH4 *10
N2 *10
SO4
F
G
H
I
J
x 10^4
x 10^4

Bull and Taillefert (2001). Down to a depth of about 10 cm, precipitation of FeS prevents the accumulation of high levels of dissolved sulfide (Fig. 2D). The effects of irrigation are also clearly visible in the distributions of sulfate and the various dissolved products of organic matter breakdown (Fig. 2G–J). In particular, the concave up shapes of the average vertical profiles of ammonium, DIC and sulfide are frequently observed in irrigated nearshore sediments (e.g., Furukawa *et al.,* 2000).

b. Irrigation coefficients

With the exception of Fe^{2+} and NO_3^-, the general shape of the bioirrigation coefficient profiles is similar for the various solutes, with a fairly constant α in the upper sediment and a rapid drop-off to zero at about 15 cm depth (Fig. 3). This shape reflects the constant burrow surface exchange area over the 0–15 cm depth interval. The absolute α values, however, differ substantially from one solute to another. The irrigation coefficient α_{O_2} exceeds all others, partly because of the large molecular diffusion coefficient of O_2 (Table 1), but also because of the high reactivity of O_2, which results in steep concentration gradients at the burrow-sediment interface. Intermediate α values are observed for TS, NH_4^+, DIC, N_2 and sulfate.

Eq. 3 indicates that the irrigation coefficient is proportional to the molecular diffusion coefficient (Christensen *et al.,* 1984). Differences in diffusion coefficients alone cannot explain the variations of α among the solute species, however. For instance, the irrigation coefficients of N_2 and DIC differ by more than a factor of 2 (Fig. 3), but only about 75% of this difference can be attributed to the larger diffusion coefficient of N_2 (Table 1). The remainder reflects the difference in location of production of the two species. Production of N_2 is stimulated locally near the burrow wall through denitrification coupled to nitrification, thereby creating a steeper radial concentration gradient, and hence a larger value of α for N_2 than for DIC (Eq. 3). The higher diffusion coefficient of ammonium compared to DIC (Table 1) is partially balanced by NH_4^+ removal via nitrification in the oxic zone adjacent to the burrow wall. As a consequence the resulting α values for NH_4^+ and DIC are similar. For Fe^{2+}, oxidative removal is so fast that almost no Fe^{2+} reaches the burrow, resulting in a near-zero irrigation coefficient (Fig. 3).

As a result of nitrification, fueled by vertical and lateral penetration of O_2 into the sediment, NO_3^- exhibits a concentration maximum in the vicinity of the burrow wall and the SWI (Fig. 2C). The NO_3^- concentration gradient near these interfaces therefore causes

←

Figure 2. Steady state solute concentration fields for a permanently flushed burrow. Panels A and F show horizontally averaged depth profiles of solute concentrations, as would be measured on core slices or with diffusion equilibrators (peepers), for instance. Panels B–E display the radial concentration fields of O_2, NO_3^-, TS and Fe^{2+}. The origin of the horizontal axis corresponds to the central axis of the burrow. Panels G–J display the radial concentration fields of DIC, NH_4^+, N_2 and SO_4^{2-}, respectively.

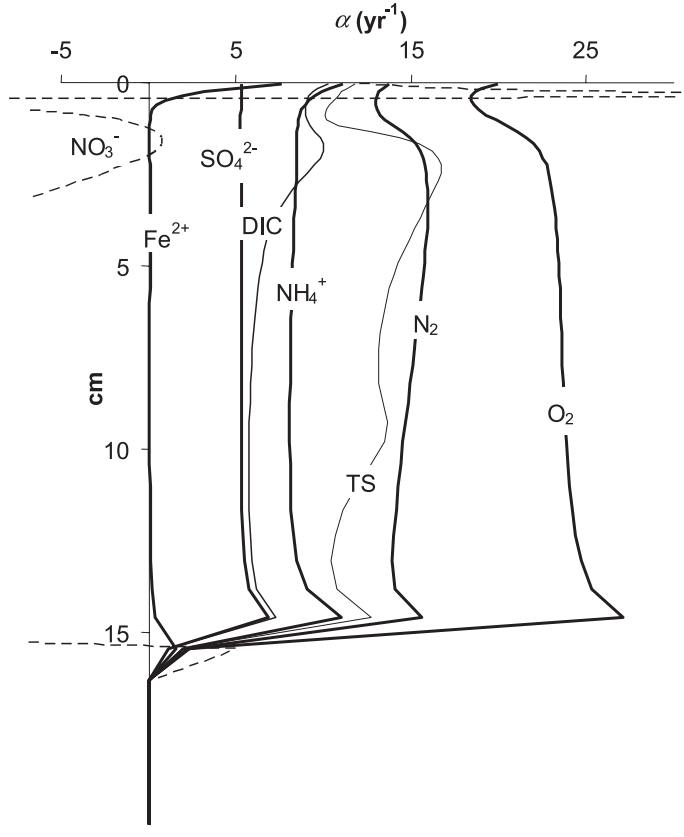

Figure 3. Depth profiles of solute-specific bioirrigation coefficients, α, for the permanently flushed burrow (baseline simulation).

an efflux of nitrate from the sediment (Fig. 4A). However, at most depths, the horizontally averaged NO_3^- concentration in the bulk sediment is below that in the overlying water (Fig. 2A). Within the framework of a 1D early diagenetic model, the removal of pore water nitrate by irrigation therefore requires negative α values (Eq. 3). For the conditions considered here, the sign of the irrigation coefficient of NO_3^- is opposite to that of the other solutes over most of the upper 15 cm (Fig. 3).

c. Flushing regime

Compared to the permanently flushed burrow simulation, intermittent flushing (10 minutes flushing, 20 minutes rest) leads to a slight decrease in the time-averaged irrigation flux of O_2 and NO_3^- (Fig. 4B, diagonally dashed columns). It somewhat enhances the removal of ammonium and DIC but, similar to the findings of Boudreau and Marinelli (1993) for dissolved silica, time-averaged irrigation fluxes vary only moderately between continuous flushing and periodic flushing on sub-hourly intervals. As a result, the irrigation coefficient

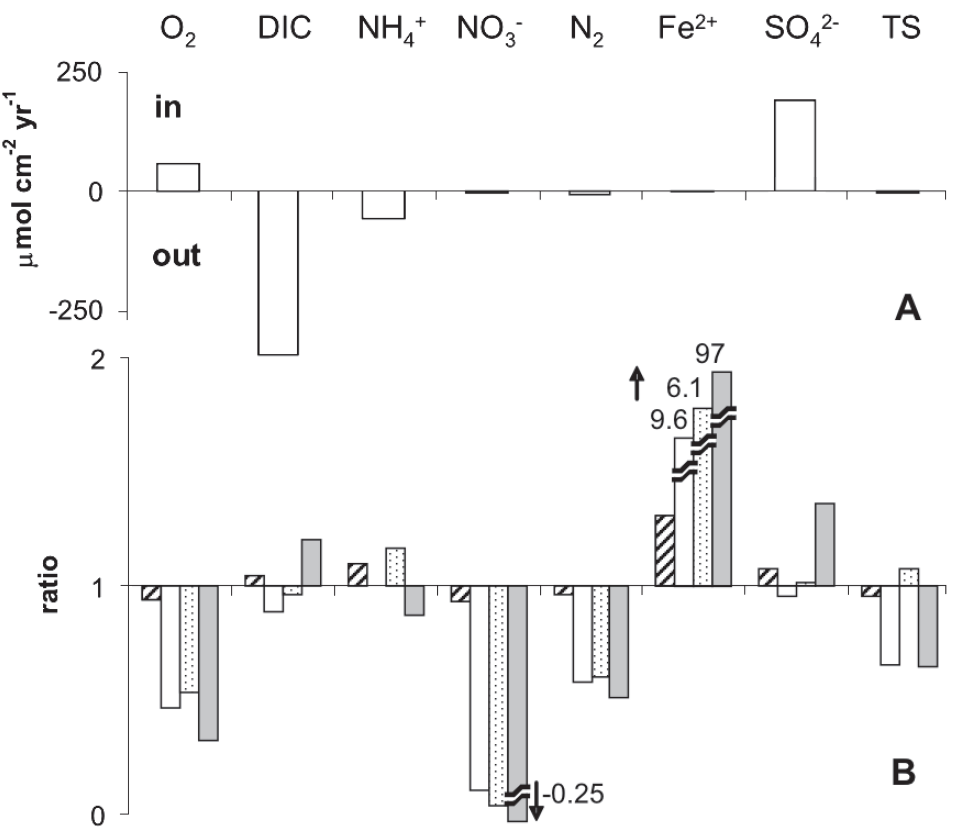

Figure 4. Irrigation fluxes for different flushing regimes and bottom water O_2 concentrations. Panel A displays the fluxes in the baseline scenario (permanent flushing). Panel B displays the changes in the fluxes for the other scenarios, relative to the baseline simulation: intermittent flushing (20 minutes rest, 10 minutes flushing; diagonally dashed columns), flushing triggered by O_2 depletion in the burrow (open columns), and permanent flushing with half the O_2 concentration in the bottom water (dotted columns). Gray columns correspond to the irrigation fluxes calculated using an average α-profile for all solute species, under a permanent flushing regime.

profiles of the permanently and intermittently flushed scenarios are similar (compare lines 1 and 2 in Fig. 5).

In the simulations, flushing triggered by a drop of the burrow O_2 concentration below 20 μM corresponds to a flushing event roughly every 2 hours. Under this flushing regime, irrigation fluxes of most species differ substantially from the permanently flushed case (Fig. 4B, open columns). The effect is particularly pronounced for O_2 whose irrigation flux drops by approximately a factor of 2, causing early diagenesis in the upper 15 cm to shift to a more anoxic regime. The resulting irrigation fluxes are comparable to the scenario where the O_2 content of the overlying water is reduced to 114 μM, i.e., half the value in the baseline scenario (Fig. 4B, dotted columns). As less O_2 is available for secondary

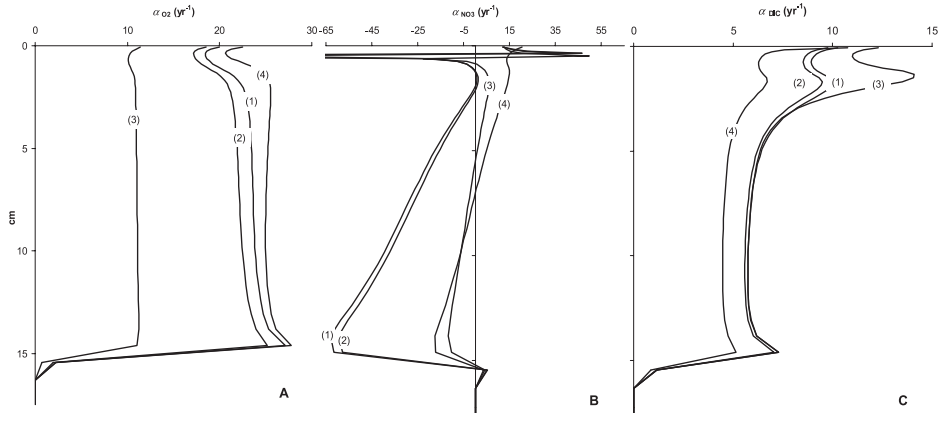

Figure 5. Panels A–C show α profiles of O_2, NO_3^- and dissolved inorganic carbon (DIC), for the following scenarios: (1) permanent flushing (baseline scenario), (2) intermittent flushing with a 20 minutes rest period alternating with 10 minutes of flushing, (3) intermittent flushing triggered by a drop in burrow O_2 concentration below 20 micromoles L^{-1}, and (4) permanent flushing with a bottom water O_2 concentration half that in the baseline simulation.

oxygenation reactions, the nitrate subsurface maximum associated with nitrification decreases and the nitrate flux out of the sediment approaches zero. Decrease of O_2 delivery and lower nitrification also reduces the production and efflux of N_2. Although the dissolved Fe^{2+} flux ratios change drastically, the absolute Fe^{2+} irrigation fluxes are negligible in all scenarios.

The flushing regime and bottom water O_2 concentration variously affect the calculated 1D irrigation coefficient profiles (Fig. 5). For O_2, the largest change in the α profile relative to the baseline simulation is seen in the scenario where flushing is triggered when the burrow O_2 concentration drops below the 20 μM O_2 threshold level. In this case, the O_2 concentration in the burrow is allowed to deviate significantly from the concentration in the overlying water. This scenario is most unlike the idealized, perfectly flushed burrow network, which underlies the simple mass transfer formulation, $\alpha(C_0 - \bar{C})$, of nonlocal irrigation. Because in the 1D representation, solute transport by irrigation is proportional to the concentration difference $(C_0 - \bar{C})$, the similar O_2 fluxes in simulations with infrequent flushing and reduced O_2 bottom water concentrations (Fig. 4B) imply a two-fold difference in the O_2 irrigation coefficients between the two scenarios (compare lines 3 and 4 in Fig. 5A). While depletion of O_2 in the burrows as well as reduced bottom water O_2 concentrations have a major impact on the α profiles of NO_3^-, the α profiles of DIC are fairly similar in the various scenarios (Fig. 5C).

d. Average and tracer irrigation coefficients

In most early diagenetic modeling applications, the same irrigation coefficient is applied to all pore water solutes. The results of this study, however, indicate that 1D reactive

transport calculation based on a single, average α profile may substantially misrepresent the role of bioirrigation in early diagenesis. This is illustrated in Figure 4B, where irrigation fluxes based on an average α profile are compared to the actual fluxes obtained using the tubular burrow model (gray columns in Fig. 4B). As average irrigation coefficient, the mean of the values for DIC and NH_4^+ is used. As can be seen in the figure, the O_2 irrigation flux in the baseline scenario is several-fold larger than that predicted using the average α profile. The relative difference in fluxes is even greater for Fe^{2+}, while for NO_3^-, use of average α-values results altogether in an opposite direction of the benthic irrigation flux. The effects for SO_4^{2-} and TS are less pronounced, as their α-profiles are closer to the average distribution.

The use of a conservative tracer avoids the interference of the early diagenetic reactivity of a solute species on the determination of its irrigation coefficient. Unreactive tracers, such as bromide, have therefore been utilized to constrain irrigation intensities in sediments (Martin and Banta, 1992). Here, we analyze tracer depth profiles predicted by the tube irrigation model, under conditions similar to those encountered in a core incubation experiment. The model simulations assume that the uptake of tracer by the sediment does not significantly decrease the tracer concentration in the overlying water. That is, the tracer is added in large excess to the overlying water.

Laterally-averaged depth profiles of the tracer obtained at different incubation times are shown in Figure 6. Also shown are the best fits of Eq. (4) to the profiles, assuming a constant value of α in the upper 15 cm. For any given incubation time, the averaged concentration profile is accurately reproduced by the 1D diffusion-irrigation model. However, the resulting irrigation coefficients are dependent on the incubation time (Fig. 6). The highest value is obtained at the very beginning of the incubation, when the concentration difference between burrow water and sediment pore water is greatest. During the first few hours of incubation, the α value of the tracer most closely resembles that of O_2. This reflects similar radial concentration gradients, with limited penetration of the solutes in the sediment surrounding the burrows. However, with continued diffusion of the tracer into the sediment, the radial tracer concentration gradient decreases, as does the value of α. After several days, the irrigation coefficient approaches a constant value, of similar magnitude as the irrigation coefficients of DIC, NH_4^+ and SO_4^{2-}. That is, with time, the tracer irrigation coefficient approaches the α values of pore water species that exhibit relatively uniform radial distributions of their net production or consumption rate.

The results of the simulations suggest that, in order to avoid transient effects on inferred irrigation coefficients, the duration of tracer incubation experiments should be sufficiently long. Long incubation times, however, may exacerbate experimental artifacts related to O_2 depletion and the build-up of toxic metabolites, which modify macrofaunal activity and, hence, pore water irrigation (Rao and Jahnke, 2004). Model simulations, such as those presented here, may assist in designing tracer incubation experiments and help with the interpretation of time-dependent tracer distributions.

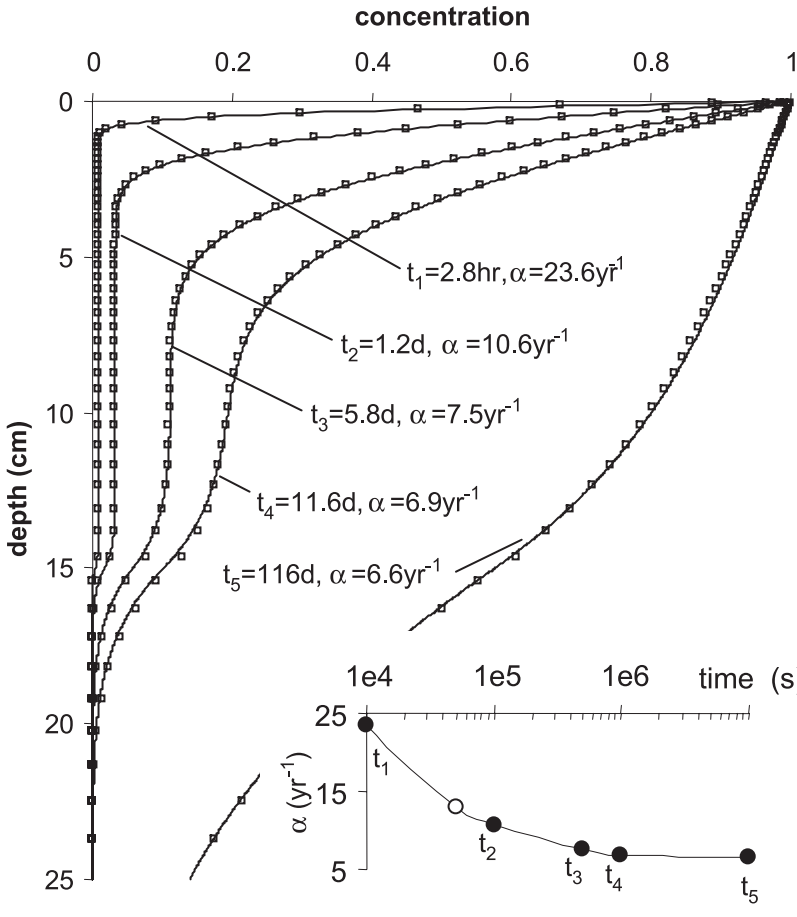

Figure 6. Time-dependent evolution of the vertical concentration profile of a conservative tracer during a core incubation experiment. At time 0, the concentration of the tracer is 0 in the sediment and 1 in the overlying water and the burrow. The symbols denote the average concentrations derived from the tube model. The lines are the corresponding profiles calculated with a 1D model (Eq. 4 in the text). The values of the optimized irrigation coefficients are indicated in the graph. Note that α is taken to be constant from time 0 to the end of each simulation, i.e. from 0 to 2.8 hrs, 0 to 1.2 days, etc. The inset shows the variation of the irrigation coefficient with time, with an asymptotic value of about 6.6 yr^{-1}. The latter value depends on the diffusion coefficient, here set to 10^{-9} m^2 s^{-1}.

e. Rates

One approach to determine *in situ* process rates is to match concentration distributions predicted by reactive transport modeling to measured ones. In sediments, vertical pore water concentration profiles are typically measured using sliced sediment cores or dialysis chambers ("peepers"). These devices integrate over horizontal scales on the order of

centimeters, and, hence, do not resolve the spatial heterogeneity in the concentration fields due to the presence of burrows. Horizontal heterogeneity of the concentrations of reactants and products of biogeochemical reactions may have a significant effect on inferred vertical rate distributions. This is illustrated here by computing vertical rate profiles from the results of the radially symmetric tube model, in the following two ways. First, the reaction rate, $\bar{R}(z)$, is obtained for each depth interval $[z, z + \Delta z]$ by averaging the rate over all the grid cells in the interval (taking into account the variable volumes of the cells). That is, $\bar{R}(z)$ represents the true radial average of the (microscopic) reaction rate distribution in the burrowed sediment. Second, the apparent rate $R(\bar{C}(z))$ at depth z is calculated using the horizontally averaged concentrations. In computing $\bar{R}(z)$ and $R(\bar{C}(z))$, the same reaction rate expressions and rate parameters are used (Table 1). The vertical rate distribution $R(\bar{C}(z))$ is thus the one that would result from a 1D early diagenetic model matching the measured vertical concentration profiles.

The vertical profiles of $\bar{R}(z)$ and $R(\bar{C}(z))$ for Fe^{2+} oxygenation and net ammonium production are shown in Figure 7. While the profile of $\bar{R}(z)$ indicates that substantial Fe^{2+} oxygenation is restricted to the uppermost two centimeters, the apparent rate distribution $R(\bar{C}(z))$ predicts that the reaction extends much deeper in the sediment. Furthermore, the depth-integrated rate of iron oxidation by O_2 obtained from $R(\bar{C}(z))$ is significantly higher than the actual integrated rate. Use of the horizontally averaged Fe^{2+} and O_2 concentrations results in an overestimation of the rate, because $R(\bar{C}(z))$ does not take into account the horizontal separation of the two reactants (Fig. 2). The discrepancy between $\bar{R}(z)$ and $R(\bar{C}(z))$ is less pronounced in the top centimeter, where vertical variations in the concentrations exceed their radial variations. The situation is even worse for NH_4^+. Because of vertical overlap of the horizontally averaged NH_4^+ and O_2 concentrations, $R(\bar{C}(z))$ erroneously suggests net NH_4^+ consumption over the entire depth range of irrigation (Fig. 7). In fact, the actual rate distribution indicates that production of ammonium by organic matter breakdown exceeds nitrification in the model sediment.

Chemical heterogeneity caused by burrowing macrofauna represents a major hurdle for the representation and parameterization of reaction kinetics in 1D early diagenetic models. Kinetic expressions and rate parameters are mostly obtained from laboratory experiments or sediment incubations where spatial heterogeneity is minimized by mechanical means. These expressions and parameters are, strictly speaking, only appropriate for implementation in 3D reactive transport models and cannot simply be extrapolated to a 1D model. As an example, consider nitrification, which is represented in the model by a bimolecular rate expression with a "true" rate constant, k_{nitri} (R_5 in Table 1). This rate constant can be compared to the apparent (or effective) 1D coefficient, defined as $k_{eff}(z) = \bar{R}_5/(\overline{O_2 NH_4^+})$, which correctly reproduces the "true" horizontally-averaged reaction rate from the horizontally-averaged reactant concentrations. Near the SWI, where vertical diffusion is dominant, k_{eff} is approximately equal to k_{nitri} (not shown). However, because of the horizontal separation of the reactants in depth interval 2–15 cm (Figs. 2B and 2H), k_{eff} drops to about 25% of the true rate constant for nitrification (not shown). For the oxygenation of Fe^{2+}, the

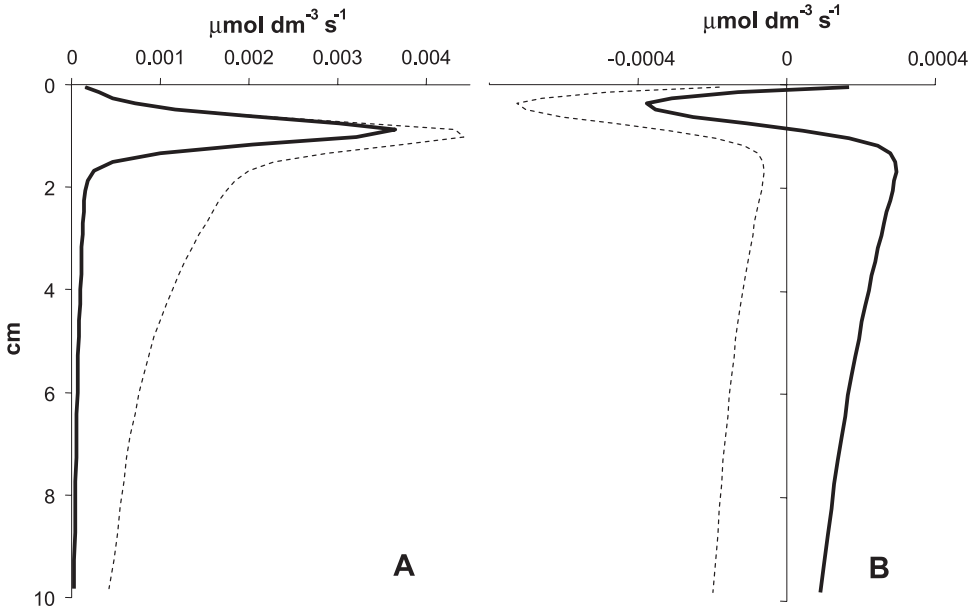

Figure 7. Depth profiles of the rates of Fe^{2+} oxygenation (panel A) and net production of NH_4^+ (panel B). Solid lines represent the true, horizontally averaged rates, $\bar{R}(z)$, while dashed lines represent rates calculated from the horizontally averaged concentrations, $R(\bar{C}(z))$. Positive rates denote Fe^{2+} consumption (A), and ammonium production (B). Rates are calculated according to the kinetics and stoichiometries given in Table 1. See text for complete discussion.

apparent 1D rate coefficient in this depth interval is even less than 10% of the assumed true value of the rate constant.

4. Conclusions

In one-dimensional (1D) reactive transport models of sediments, biologically induced solute mixing is usually represented via a vertical mass transfer or irrigation coefficient, α, whose value is a measure of the intensity of the diffusional exchange fluxes between the sediment matrix and flushed burrows. As these fluxes depend on the radial concentration gradients at the burrow-sediment interface, variable biogeochemical reactivities of pore water species are expected to result in a range of solute-specific irrigation coefficients. The explicit modeling of three-dimensional concentration and rate distributions around a vertical burrow indeed demonstrates that α values vary substantially from one reactive solute to another. In the case of nitrate, even the sign of the irrigation coefficient may differ from that of the other solutes. Thus, the use of an average α profile for all pore water species in 1D early diagenetic models is likely to introduce significant errors in predicted solute fluxes and reaction rates.

Simulation of the uptake of an inert tracer during a core incubation experiment also

yields nonunique irrigation coefficients, because of the temporal evolution of the radial tracer concentration gradient away from the burrow wall. Consequently, for short incubation times, and hence steep radial and vertical concentration gradients, the tracer irrigation coefficient is representative of highly reactive solutes supplied from the overlying water, such as molecular oxygen. For long incubation times, the tracer irrigation coefficient approaches those of dissolved inorganic carbon, sulfate and ammonium; that is, solutes that exhibit more gradual vertical and radial concentration gradients in the irrigated zone of the sediment. These results indicate that it may be possible to use transient tracer distributions to constrain the expected range of irrigation coefficients of reactive species.

The three-dimensional chemical dynamics created by the presence and flushing of burrows not only influence the irrigation coefficients of solute species, but also the representation of reaction kinetics in 1D early diagenetic models. Apparent 1D reaction rates and reaction parameters may deviate significantly from their three-dimensional equivalents. In particular, as 1D early diagenetic models do not account for the horizontal redox zonation in irrigated sediments, apparent rate constants for redox transformations based on horizontally averaged concentrations are, in general, smaller than the true (microscopic) values. More complex situations arise, however, for redox species that are both produced and consumed within the same depth interval, as may be the case for nitrate and ammonium. Thus, as for the irrigation coefficients, the kinetic scaling effects are strongly dependent on the biogeochemical reactivities of the species involved.

Our results illustrate that a fundamental understanding of transport and reaction processes at the level of individual burrows may help the parameterization of 1D reactive transport models of sediments. Within the foreseeable future, the latter are likely to remain the major quantitative tool for analyzing the predominantly vertical data sets that are being collected as part of early diagenetic studies. It is therefore crucial to identify the potential pitfalls of representing inherently three-dimensional processes in 1D models. As an outcome of this study, we recommend allowing for inter-species differences in irrigation coefficients. The differences in α profiles shown in Figure 3 may serve as a rough guide of the expected relative variations in irrigation coefficients among reactive early diagenetic solutes.

Acknowledgments. This study was supported by the Netherlands Organisation for Scientific Research (NWO, Pioneer Programme), the Shared University Research Grants from IBM Inc. to Indiana University and the IBM Life Sciences Institutes of Innovations. We thank Don Rice, Bill Martin and an anonymous reviewer for providing helpful and constructive comments.

REFERENCES

Aller, R. C. 1980. Quantifying solute distributions in the bioturbated zone of marine sediments by defining an average microenvironment. Geochim. Cosmochim. Acta, *44,* 1955–1965.

—— 1983. The importance of the diffusive permeability of animal burrow linings in determining marine sediment chemistry. J. Mar. Res., *41,* 299–322.

—— 2001. Transport and reactions in the bioirrigated zone, *in* The Benthic Boundary Layer, B. P. Boudreau and B. B. Jørgensen, eds., Oxford University Press, 269–301.

Balzer, W. 1982. On the distribution of iron and manganese at the sediment/water interface: thermodynamic versus kinetic control. Geochim. Cosmochim. Acta, *46,* 1153–1161.

Berg, P., N. Risgaard-Petersen and S. Rysgaard. 1998. Interpretation of measured concentration profiles in the sediment porewater. Limnol. Oceanogr., *43,* 1500–1510.

Berg, P., S. Rysgaard and B. Thamdrup. 2003. Dynamic modeling of early diagenesis and nutrient cycling. A case study in an arctic marine sediment. Am. J. Sci., *303,* 905–955.

Boudreau, B. P. 1984. On the equivalence of nonlocal and radial-diffusion models for porewater irrigation. J. Mar. Res., *42,* 731–735.

—— 1996. A method-of-lines code for carbon and nutrient diagenesis in aquatic sediments. Computers Geosci., *22,* 479–496.

—— 1997. Diagenetic Models and Their Implementation, Springer, 414 pp.

Boudreau, B. P. and R. Marinelli. 1993. Effects of discontinuous vs. continuous irrigation on dissolved silica fluxes from marine sediments. Chem. Geol., *107,* 439–441.

Brendel, P. J. 1995. Development of a mercury thin film voltametric microelectrode for the determination of biogeochemically important redox species in porewaters of marine and freshwater sediments. PhD Thesis, University of Delaware.

Bull, D. C. and M. Taillefert. 2001. Environmental and seasonal variations in porewaters of a southeastern USA salt marsh as revealed by voltammetric microelectrode profiling. Geochem. Trans., *13,* 1–8.

Christensen, J. P., A. H. Devol and W. M. Smethie. 1984. Biological enhancement of solute exchange between sediments and bottom water on the Washington continental shelf. Cont. Shelf Res., *3,* 9–23.

Emerson, S., R. Jahnke and D. Heggie. 1984. Sediment-water exchange in shallow water estuarine sediments. J. Mar. Res., *42,* 709–730.

Fossing, H., T. G. Ferdelman and P. Berg. 2000. Sulfate reduction and methane oxidation in continental margin sediments influenced by irrigation (South-East Atlantic off Namibia). Geochim. Cosmochim. Acta, *64,* 897–910.

Furukawa, Y. 2001. Biogeochemical consequences of macrofauna burrow ventilation. Geochem. Trans., *11,* DOI: 10.1039/b108381c.

Furukawa, Y., S. J. Bentley and D. L. Lavoie. 2001. Bioirrigation modeling in experimental benthic mesocosms. J. Mar. Res., *59,* 417–452.

Furukawa, Y., S. J. Bentley, A. M. Shiller, D. L. Lavoie and P. Van Cappellen. 2000. The role of biologically-enhanced pore water transport in early diagenesis: An example from carbonate sediments in the vicinity of North Key Harbor, Dry Tortugas National Park, Florida. J. Mar. Res., *58,* 493–522.

Gilbert, F., R. C. Aller and S. Hulth. 2003. The influence of macrofaunal burrow spacing and diffusive scaling on sedimentary nitrification and denitrification: An experimental simulation and model approach. J. Mar. Res., *61,* 101–125.

Gribsholt, B., J. E. Kostka and E. Kristensen. 2003. Impact of fiddler crabs and plant roots on sediment biogeochemistry in a Georgia saltmarsh. Mar. Ecol. Progr. Ser., *259,* 237–251.

Heip, C. H. R., G. Duineveld, E. Flach, G. Graf, W. Helder, P. M. J. Herman, M. Lavaleye, J. J. Middelburg, O. Pfannkuche, K. Soetaert, T. Soltwedel, H. de Stigter, L. Thomsen, J. Vanaverbeke and P. de Wilde. 2001. The role of the benthic biota in sedimentary metabolism and sediment-water exchange processes in the Goban Spur area (NE Atlantic). Deep-Sea Res. II, *48,* 3223–3243.

Koretsky, C. M., C. Meile and P. Van Cappellen. 2002. Quantifying bioirrigation using ecological parameters: a stochastic approach. Geochem. Trans., *3,* 17–30.

Kristensen, E. 2000. Organic matter diagenesis at the oxic/anoxic interface in coastal marine sediments, with emphasis on the role of burrowing animals. Hydrobiol., *426,* 1–24.

Marinelli, R. L., C. R. Lovell, S. G. Wakeham, D. B. Ringelberg and D. C. White. 2002.

Experimental investigation of the control of bacterial community composition in macrofaunal burrows. Mar. Ecol. Progr. Ser., *235,* 1–13.

Martin, W. R. and G. T. Banta. 1992. The measurements of sediment irrigation rates: a comparison of the Br^- tracer $^{222}Rn/^{226}Ra$ disequilibrium techniques. J. Mar. Res., *50,* 125–154.

Martin, W. R. and F. L. Sayles. 1987. Seasonal cycles of particulate and solute transport processes in nearshore sediments: $^{222}Rn/^{226}Ra$ and $^{234}Th/^{238}U$ disequilibrium at a site in Buzzards Bay, MA. Geochim. Cosmochim. Acta, *51,* 927–943.

Mayer, M. S., L. Schaffner and W. M. Kemp. 1995. Nitrification potentials of benthic macrofaunal tubes and burrow walls: effects of sediment NH_4^+ and animal irrigation behavior. Mar. Ecol. Progr. Ser., *121,* 157–169.

Meile, C., C. M. Koretsky and P. Van Cappellen. 2001. Quantifying bioirrigation in Aquatic sediments: An inverse modeling approach. Limnol. Oceanogr., *46,* 164–177.

Meile, C., K. Tuncay and P. Van Cappellen. 2003. Explicit representation of spatial heterogeneity in reactive transport models: Application to bioirrigated sediments. J. Geochem. Explor., *78–79,* 231–234.

Meile, C. and P. Van Cappellen. 2003. Global estimates of enhanced solute transport in marine sediments. Limnol. Oceanogr., *48,* 777–786.

Nielsen, O. I., B. Gribsholt, E. Kristensen and N. P. Revsbech. 2004. Microscale distribution of oxygen and nitrate in sediment inhabited by *Nereis diversicolor:* spatial patterns and estimated reaction rates. Aquat. Microb. Ecol., *34,* 23–32.

Nielsen, O. I., E. Kristensen and M. Holmer. 2003. Impact of *Arenicola marina* (Polychaeta) on sediment sulfur dynamics. Aquat. Microb. Ecol., *33,* 95–105.

Patankar, S. V. 1980. Numerical Heat Transfer and Fluid Flow, Taylor & Francis, 197 pp.

Pelegri, S. P., L. P. Nielsen and T. H. Blackburn. 1994. Denitrification in estuarine sediment stimulated by the irrigation activity of the amphipod *Corophium volutator.* Mar. Ecol. Progr. Ser., *105,* 285–290.

Rao, A. M. F. and R. A. Jahnke. 2004. Quantifying pore water exchange across the sediment water interface in the deep sea with *in situ* tracer studies. Limnol. Oceanogr. Methods, *2,* 75–90.

Rysgaard, S. and P. Berg. 1996. Mineralization in a northeastern Greenland sediment: mathematical modelling, measured sediment pore water profiles and actual activities. Aquat. Microb. Ecol., *11,* 297–305.

Steward, C. C., S. C. Nold, D. B. Ringelberg, D. C. White and C. R. Lovell. 1996. Microbial biomass and community structure in the burrows of bromophenol producing and nonproducing marine worms and surrounding sediments. Mar. Ecol. Progr. Ser., *133,* 149–165.

Sundby, B., L. G. Anderson, P. O. J. Hall, Å. Iverfeldt, M. M. Rutgers van der Loeff and S. F. G. Westerlund. 1989. The effect of oxygen on release and uptake of cobalt, manganese, iron and phosphate at the sediment-water interface. Geochim. Cosmochim. Acta, *50,* 1281–1288.

Van Cappellen, P. and Y. Wang. 1996. Cycling of iron and manganese in surface sediments: A general theory for the coupled transport and reaction of carbon, oxygen, nitrogen, sulfur, iron, and manganese. Am. J. Sci., *296,* 197–243.

Wang, Y. and P. Van Cappellen. 1996. A multicomponent reactive transport model of early diagenesis: Application to redox cycling in coastal marine sediments. Geochim. Cosmochim. Acta, *60,* 2993–3014.

Received: *18 June, 2004;* revised: *13 January, 2005.*